REPORT DOCUMENTATION PAGE

Form Approved
OMB No. 0704-0188

PLEASE DO NOT RETURN YOUR FORM TO THE ABOVE ADDRESS.

1. REPORT DATE *(DD-MM-YYYY)*	2. REPORT TYPE	3. DATES COVERED *(From - To)*
22-02-2011	Reprint	Jan 2005 - Sept 2010

4. TITLE AND SUBTITLE

Locally adaptive detection algorithm for forward-looking ground-penetrating radar

5a. CONTRACT NUMBER

W911NF-05-1-0069

5b. GRANT NUMBER

5c. PROGRAM ELEMENT NUMBER

6. AUTHOR(S)

Havens, Tim, C.
Ho, Dominic, K.C.
Farrell, Justin
Keller, James, M.
Popescu, Mihail
Ton, Tuan, T.
Wong, David, C.

5d. PROJECT NUMBER

5e. TASK NUMBER

5f. WORK UNIT NUMBER

7. PERFORMING ORGANIZATION NAME(S) AND ADDRESS(ES)

University of Missouri
Office of Research
205 Jesse Hall
Columbia, MO 65211

8. PERFORMING ORGANIZATION REPORT NUMBER

9. SPONSORING/MONITORING AGENCY NAME(S) AND ADDRESS(ES)

Department of the Army
US Army Research, Development and Engineering Command Acquisition Center
Research Triangle Park Contracting Division
P.O. Box 12211
Research Triangle Park, NC 27709-2211

10. SPONSOR/MONITOR'S ACRONYM(S)

ARO Terrestrial Sciences

11. SPONSOR/MONITOR'S REPORT NUMBER(S)

12. DISTRIBUTION/AVAILABILITY STATEMENT

Approved for public release; federal purpose rights.

13. SUPPLEMENTARY NOTES

14. ABSTRACT

This paper proposes an effective anomaly detection algorithm for a forward-looking ground-penetrating radar (FLGPR). One challenge for threat detection using FLGPR is its high dynamic range in response to different kinds of targets and clutter objects. The application of a fixed threshold for detection often yields a large number of false alarms. We propose a locally-adaptive detection method that adjusts the detection criteria automatically and dynamically across different spatial regions, which improves the detection of weak scattering targets. The paper also examines a spectrum based classifier. This classifier rejects false alarms (FAs) by classifying each alarm location based on its spatial frequency-spectrum. Experimental results for the improved detection techniques are demonstrated by field data measurements from a US Army test site.

15. SUBJECT TERMS

Forward-Looking Explosive Hazards Detection, Ground-Penetrating Radar, Spatial Frequency, False Alarm Rejection, One-Class Classifiers

16. SECURITY CLASSIFICATION OF:			17. LIMITATION OF ABSTRACT	18. NUMBER OF PAGES	19a. NAME OF RESPONSIBLE PERSON
a. REPORT	b. ABSTRACT	c. THIS PAGE			Jim Keller
UU	UU	UU	UU	9	19b. TELEPHONE NUMBER *(Include area code)* (573) 882-7339

Reset

Locally-Adaptive Detection Algorithm for Forward-Looking Ground-Penetrating Radar

Timothy C. Havens*[a], K.C. Ho[a], Justin Farrell[a], James M. Keller[a], Mihail Popescu[a],
Tuan T. Ton[b], David C. Wong[b], and Mehrdad Soumekh[c]
[a]Dept. of Electrical and Computer Engineering, University of Missouri, Columbia, MO, USA 65211;
[b]U.S. Army Night Vision & Electronic Sensors Directorate, Fort Belvoir, Virginia, USA 22060;
[c]Dept. Of Electrical Engineering, University of New York at Buffalo, Amherst, NY, USA 14260

ABSTRACT

This paper proposes an effective anomaly detection algorithm for a *forward-looking ground-penetrating radar* (FLGPR). One challenge for threat detection using FLGPR is its high dynamic range in response to different kinds of targets and clutter objects. The application of a fixed threshold for detection often yields a large number of false alarms. We propose a locally-adaptive detection method that adjusts the detection criteria automatically and dynamically across different spatial regions, which improves the detection of weak scattering targets. The paper also examines a spectrum-based classifier. This classifier rejects *false alarms* (FAs) by classifying each alarm location based on its spatial frequency-spectrum. Experimental results for the improved detection techniques are demonstrated by field data measurements from a US Army test site.

Keywords: Forward-looking explosive hazards detection, ground-penetrating radar, spatial frequency, false alarm rejection, one-class classifiers

1. INTRODUCTION

Remediation of the threat of explosive hazards is an extremely important goal, as these hazards are responsible for uncountable deaths and injuries to both civilians and soldiers throughout the world. Systems that detect explosive hazards have included *ground-penetrating-radar* (GPR), *infrared* (IR) cameras, and acoustic technologies.[1-3] Both handheld and vehicle-mounted GPR-based systems have been examined in recent research and much progress has been made in increasing detection capabilities.[4,5] *Forward-looking* synthetic aperture GPR (FLGPR) is an especially attractive technology because of its ability to detect hazards before they are encountered; standoff distance can range from a few to tens of meters. FLGPR has been applied to the detection of side-attack mines[6], and mines in general.[7,8] A drawback to these systems is that FLGPR is not only sensitive to objects of interest, but also to other objects, both above and below the ground. This results in an excessive number of FAs.

The FLGPR images we present in this paper were collected by a system called ALARIC. This system is an FLGPR system that is composed of a physical array of sixteen receivers and two transmitters. In the past decade, FLGPR systems have primarily used their physical arrays (aperture) as well as their radar bandwidth for imaging (resolution); conventional backprojection or time domain correlation imaging has been used for this purpose. Those FLGPR systems rarely tried to exploit imaging information that is created by the motion of the platform. The ground-based FLGPR community has referred to imaging methods that leverage platform motion as multi-look imaging. Though in the airborne radar community, this is better known as *synthetic aperture radar* (SAR) imaging. SAR has been shown to be an effective tool for airborne *intelligence, surveillance* and *reconnaissance* (ISR) applications.

The ALARIC system is equipped with an accurate GPS system. As a result, we are capable of processing both physical and synthetic aperture imaging even when the platform moves along a nonlinear path with variations in its heading. To create the FLGPR images we use a nonlinear processing technique called *Adaptive Multi-Transceiver Imaging*. This method exploits a measure of similarity among the 32 T/R images which adaptively suppresses artifacts such as sidelobes and aliasing ghots.

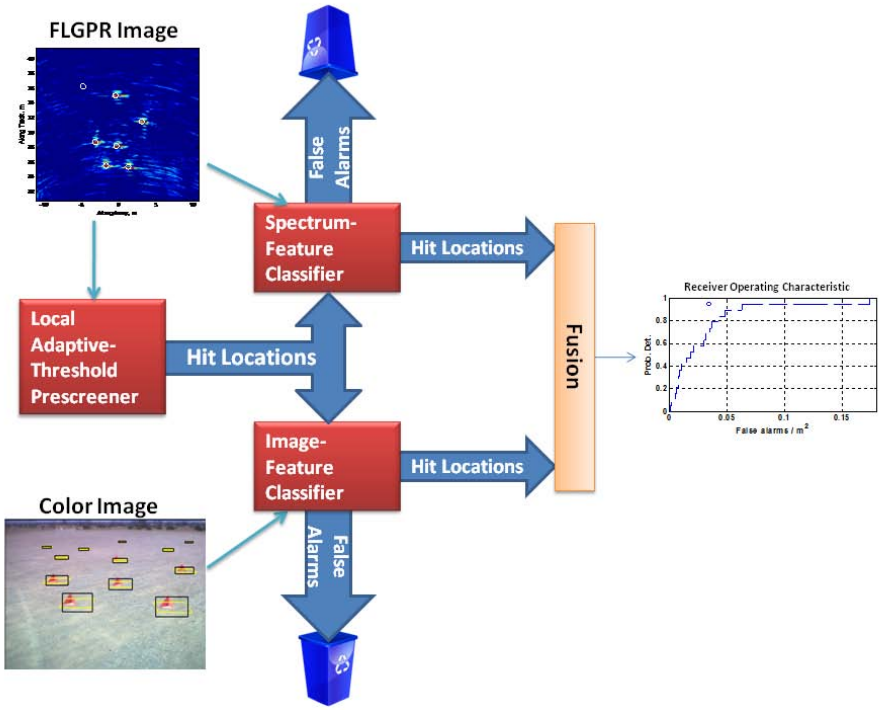

Fig. 1. Block diagram of our forward-looking explosive hazards detection algorithms. This paper focuses on the local-adaptive threshold prescreener and the spectrum-feature classifier. The image-feature classifier and fusion are described in references [9-11].

Figure 1 illustrates our proposed explosive-hazard detection algorithm. The sensor fusion with the camera-based sensor is described in references [9-11]. In this paper we focus on the locally-adaptive threshold prescreener and the spectrum-feature one-class classifier. We first propose a locally-adaptive detection algorithm. This algorithm builds upon the prescreener that we previously developed.[10,15] Unlike a conventional threshold-based detector, our algorithm detects local-maxima by applying an adaptive threshold that is sensitive to local noise levels. Test results show that this method reduces the number of FAs by 75%, as compared to a hard threshold-based method, at a probability of detection of 94%. The second algorithm we propose is a classifier that rejects FAs by characterizing the spatial spectrum of FAs. At each alarm-location we compute a 50-bin windowed *fast Fourier transform* (FFT) of the real-part of the FLGPR image. We then train a one-class classifier on these spectrum-based features. We show that we can train a generalized classifier, which is effective at reducing the number of FAs in both training data and test data. Our final results show that we can achieve an approximate FA rate of 0.03 FA/m^2 at a >90% probability of detection.

Section 2 describes the locally-adaptive detection algorithm, while in Section 3 we propose our spectrum-feature and one-class classifier for rejecting FAs. We present both training and test results in Section 4 and describe a method by which we can create a generalized classifier for rejecting FAs based on the spectrum-features. Section 5 summarizes this paper.

2. LOCALLY-ADAPTIVE THRESHOLD DETECTION ALGORITHM

The FLGPR images are created for an area -11m to 11m in the cross-range direction (although, in practice, only a sub-region of this is used in our detection algorithms), where negative numbers indicate to the left of the vehicle. Coherent integration of radar scans is performed in an area 9m to 25m in front of the vehicle. The pixel-resolution of the FLGPR image is 0.05m x 0.05m. The nominal center frequency is 1.2GHz and the bandwidth is 1.5GHz. We chose a detection region 9m wide. If the targets are on the left side of the road (relative to the vehicle) this region is positioned from -7m to +2m; if the targets are on the right side of the road this region is positioned from -2m to +7m. References [10,15] describe our previous efforts in detecting land mines in FLGPR data. The prescreener algorithm we present in this paper is an extension of this previous work.

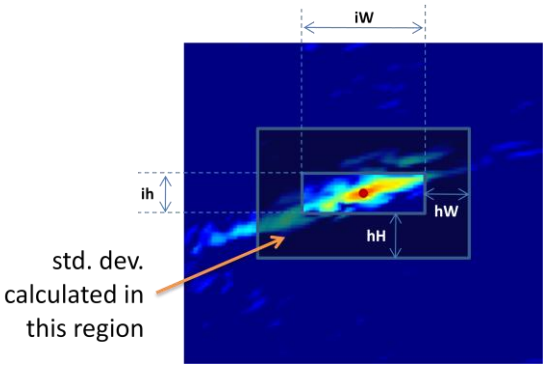

Fig. 2. Local adaptive-threshold prescreener calculates standard deviation in rectangular halo around each radar image pixel.

2.1 Detection algorithm

Consider an FLGPR image , where *u* is the cross-range coordinate and *v* is the down-range coordinate. We first filter *G* with a locally-adaptive standard deviation filter. This computes the local standard deviation in a variable-size rectangular halo around each pixel. Figure 2 shows the region in which the local standard deviation is calculated. We define this region by the dimensions of the inner rectangle and the width of the outer halo. Each pixel in is divided by the local standard deviation

_____ ,

where is the standard-deviation of the pixels within the halo region around .

The filtered image is then input to a local-maxima finding algorithm. Our detection method first computes a

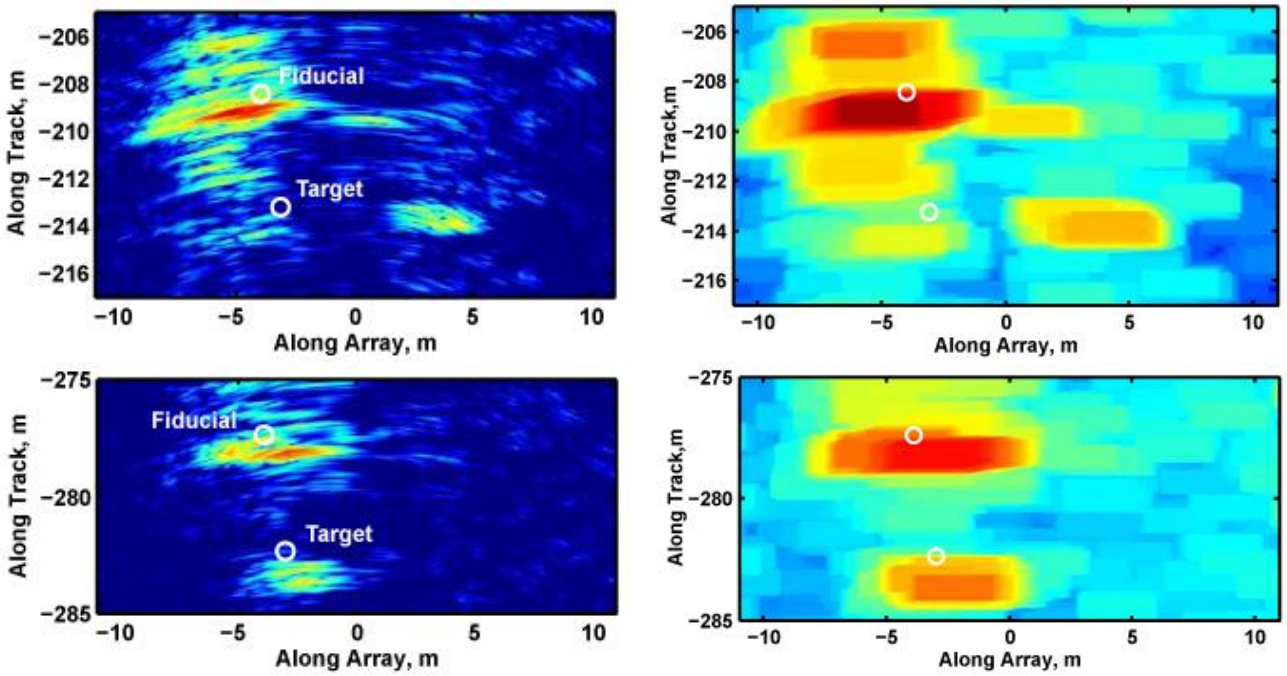

(a) Local standard-deviation filtered images

(b) Maximum order-filtered images

Fig. 3. Maximum order-filtered images of FLGPR images – target locations indicated by white circles.

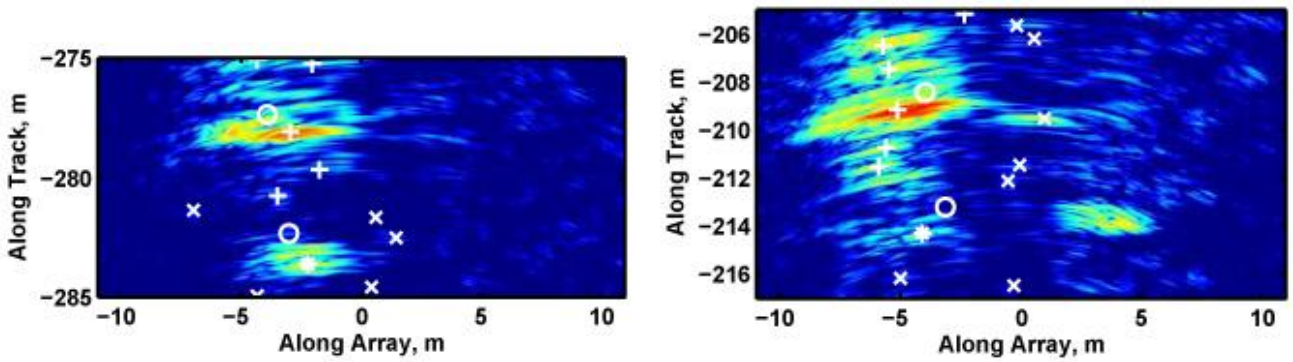

Fig. 4. Alarm locations for example images in test run 188. x indicates FA, + indicates fiducial alarm, and * indicates a target alarm.

maximum order-filtered image with a 3m x 1.5m kernel. We denote this order-filtered image as . Essentially, each pixel in the scan image is replaced by the maximum pixel value within a 3m crossrange by 1.5m downrange rectangle. Figure 3 shows two examples of FLPR images and their associated order-filtered images. As this figure shows, the order-filter reduces the noise-induced artifacts in the image and shows the local maxima as large squares in the image. Alarms are identified by the operation

,

where A is the set of local-maxima locations. The minimum operator prescreens alarm locations that have a very low FLGPR return. We choose a value of -60dB for this threshold as this only eliminates alarms with the lowest of confidence (note that the minimum value in the color scale in Fig. X is -8dB). This prescreening threshold merely minimizes the computational cost of the subsequent algorithms by reducing the number alarms to a manageable number. We also augment each alarm location (u,v) in A with the value of the FLGPR image pixel at that location, which we denote as . This pixel value is, in effect, the confidence of the alarm – the higher the pixel value (FLGPR return), the higher the confidence. Figure 4 shows the associated alarm locations of the images shown in Fig. 3.

As Figs. 3 and 4 show, there were fiducials (markers) placed near the target locations in the tests. We identified fiducial hits and removed them from our ROC calculations. The fiducial hits in Fig. 4 are denoted by the '+' symbol. Note that our method for identifying fiducial hits is not perfect, but adding or subtracting one alarm location only negligibly affects the overall ROC results.

2.2 Detection results

Figure 5 displays the effectiveness of our locally-adaptive threshold detection algorithm. The solid blue line indicates

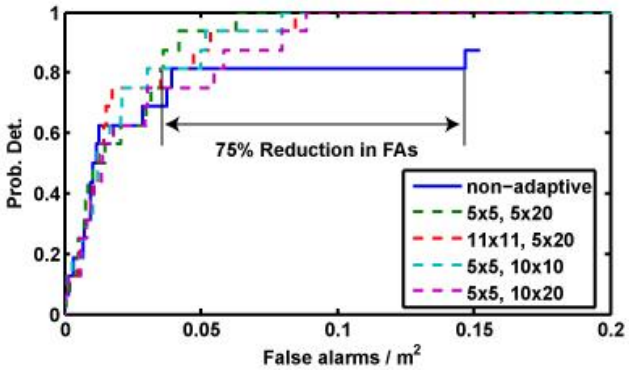

Fig. 5. ROC curve of MUFL prescreener for non-filtered radar image and three different sized locally-adaptive filter halos. The size of the rectangular halo is denoted as **iW**x**iH**, **hW**x**hH**, as shown in Fig. 2

the performance of a non-adaptive conventional threshold detector. As the ROC curve shows, this algorithm detects only 88% of the targets at a FA rate of 0.16 FA/m^2. The dotted lines indicate the performance of our locally-adaptive algorithm for four different sized windows (see Fig. 2 for an illustration of the window size). The 5x5, 5x20 window size achieved the best FA rate at a detection probability >90%. This window size results in a minimum FA rate of 0.045 FA/m^2 at a probability of detection of 94%. We stress that all instances of the locally-adaptive threshold detector were able to achieve a probability of detection of 100% with less than 0.1 FA/m^2. In Section 4 we present more results for our proposed approach.

3. SPECTRUM-BASED FALSE ALARM REJECTION

3.1 Spectrum-feature

A spectrum-based feature is calculated for each FLGPR detection. We first calculate a 50-bin windowed FFT of the row of pixels centered at the detection location

where W is a 50-point Hamming window and is the magnitude of the windowed-spectrum of , the 50-point horizontal slice of the FLGPR image centered at the alarm A. We use the 50-bins of as the features of a one-class classifier that is trained on the FA locations. Essentially, the one-class classifier is a model of the spectrum of the FAs.

3.2 One-class classifier

The 50 spectrum-based features and the FLGPR confidence value for each detection are used to classify the detection as either true (an explosive hazard) or false. We train a classifier by first calculating the multivariate normal distribution that best represents the feature values of the false detections for a given set of training data. Hence, the values of the false detections are assumed to be accurately represented by

,

where μ is the mean vector, Σ is the covariance matrix, and are the 50 features in . We fit the distribution parameters to the training data using the well-known maximum-likelihood estimator.[16] Once we have trained the classifier, we can use the Malanhobis-metric to determine how well a new feature vector X fits the false detection distribution, where this distance is calculated by

.

If the Malanhobis-metric $D(X)$ is large-valued, this indicates that the detection does not fit the false detection distribution and is, most likely, a true detection. Hence, a threshold T must be chosen such that a $D(X) > T$ indicates a true detection and a $D(X) \leq T$ indicates a false detection. The advantage of this method is that the threshold T can be tuned to offer an optimal tradeoff between true and false detections. Also, the distribution is trained on false detection data, of which there are many, rather than true detection data, of which there are few. Furthermore, the true detection features can be drastically different for different types and configurations of the explosive hazards, whereas the false detection features tend to more generalized.

3.3 Feature and Threshold Selection

There are a total of 50 spectrum-based features for each FLGPR detection. It is unlikely that all of these features are necessary or effective for training an optimal classifier. Additionally, given a set of features we must choose the threshold T which determines whether an input feature vector is classified as a true or false detection. We use an *exhaustive search* to find the four best features. In [10], we used a forward sequential search to determine the best N features. However, we have since discovered that with an exhaustive search can be performed relatively quickly and

produces more generalized classification results. At each iteration of the exhaustive feature selection, the threshold T is set such that each target in the training data has at least one associated detection. In this manner, the optimal T eliminates the most false detections while maintaining a P_D = 100%. Thus, the exhaustive search determines the four best features and associated classifier parameters, μ, Σ, and T. For comprehensive results on this classification scheme in regards to FLGPR and IR imagery, please refer to [11].

Figure 7(a) shows the training results of using the spectrum-based classifier on the alarm locations following the locally-adaptive threshold prescreener. The training data is Test Run 188. These results show that the classifier is able to reduce the FA rate from 0.045 FA / m^2 to 0.022 FA / m^2 – a greater than 50% reduction. We note, however, that these are resubstitution results and represent the best performance that would be expected from this classifier.

4. RESULTS

4.1 Locally-adaptive prescreener results

Figure 6 shows the ROC curves of the locally-adaptive prescreener on test runs 188 and 190. The size of the local standard-deviation filter used was 5x5, 5x20 (see Fig. 2 for an illustration of the filter dimensions), which was the most effective filter size on test run 188 (as shown in Fig. 5). All results shown in this section will use this filter size. On test run 188 our prescreener is able to achieve a minimum FA rate of 0.045 FA/m^2 at 94% probability of detection. On test run 190 the prescreener produces a minimum FA rate of 0.34 FA/m^2 at 90% probability of detection. Figure 6 shows that this prescreener not only effective on the training data (188) but also on the test data (190).

4.2 Spectrum-feature classifier results

Figure 7 outlines the FA rejection results for the one-class classifier trained with the spectrum-feature. A confidence threshold was chosen from the training data (test run 188) that resulted in a >90% classification rate with the least number of FAs. This is shown as the cyan dot in view (a) – this is the expected performance using just the locally-adaptive prescreener. As Fig. 7(a) illustrates, the FA rate of the locally-adaptive prescreener at 94% probability of detection is 0.045 FA/m^2. The red dot in view (a) shows the FA rate after the spectrum-feature classifier is applied. As this shows, the FA rate was reduced by >50% to 0.022 FA/m^2.

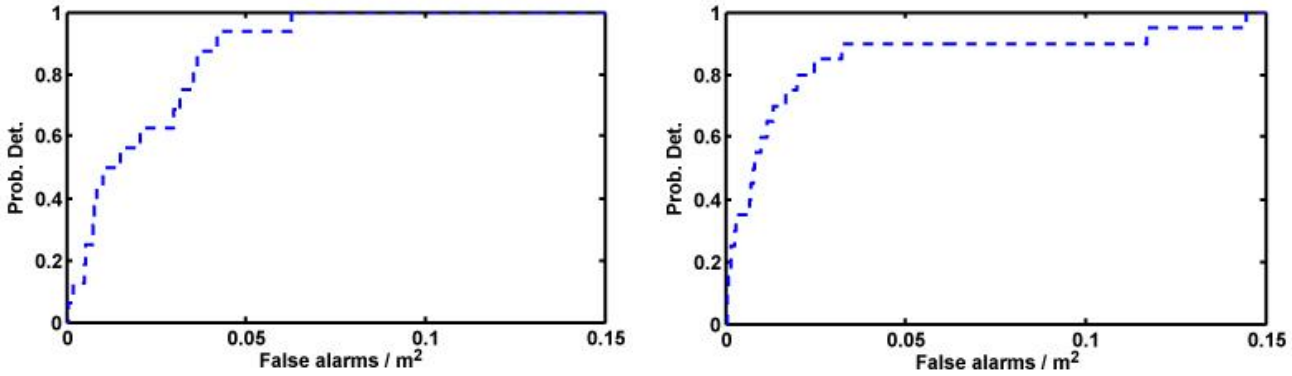

(a) ROC of test run 188

(b) ROC of test run 190

Fig. 6. Results of locally-adaptive threshold detector on test runs 188 and 190.

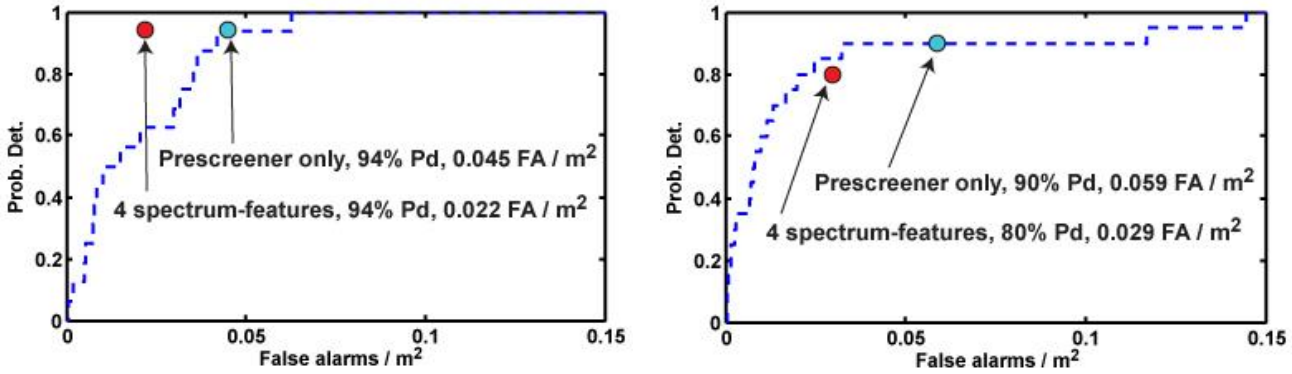

(a) Training result on test run 188

(b) Test result on test run 190

Fig. 7. Training and test results of one-class classifier with 4 spectrum-based features – bins [21,27,30,50] of FFT. Feature selection based on best training results.

The same confidence threshold was then applied to test run 190. View (b) shows that the locally-adaptive prescreener, with the threshold chosen from the training data in view (a), results in 90% probability of detection with 0.059 FA/m^2 (shown by the cyan dot). If we apply the trained spectrum-feature classifier to test run 190, we only achieve a probability of detection of 80% with a FA rate of 0.029 FA/m^2. This is clearly undesirable as the probability of detection is reduced. However, recall that only 4 of the 50 spectrum features were used in the training of the classifier. Thus, we examined other combinations (of 4 features) of the 50 spectrum features to identify features that would better generalize across the two data sets.

Figure 8 shows the results of the spectrum-feature classifier using a different set of 4 features. The 4 features were chosen that resulted in the best average training and test performance. Note that the classifier is still trained only on the training lane (188). However, by selecting a different set of features we were able to train a classifier that has a more generalized effectiveness. View (a) shows that using bins [15, 17, 30, 39] of the FFT results in a 94% probability of detection with 0.026 FA/m^2 on the lane 188 – in the pattern recognition community these are often called resubstitution results. In view (b), we show the results of the trained classifier on lane 190, the test data. With these 4 features, the classifier produces a 90% probability of detection with 0.034 FA/m^2. Although the FA rates in both the training and test data are slightly higher than those shown in Fig. 7, in contrast the test lane performance is much better as the probability of detection is maintained at 90%. These results are promising as this shows that we can build a generalized spectrum-feature classifier that significantly reduces the number of FAs in both training and test data.

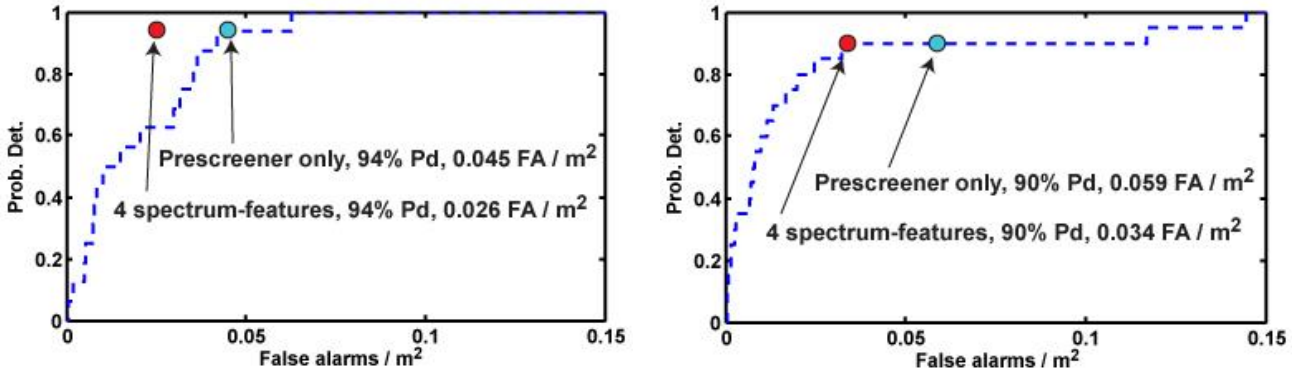

(a) Training result on test run 188

(b) Test result on test run 190

Fig. 8. Training and test results of one-class classifier with 4 spectrum-based features – bins [15,17,30,39] of FFT. Feature selection based on best average training and test results. This feature selection method results in a more generalized classifier.

4. CONCLUSION

The locally-adaptive threshold detector coupled with the spectrum-feature one-class classifier was shown to be an effective system for improving the detection capabilities of the ALARIC system. Figure 5 showed that the locally-adaptive prescreener not only enabled 100% probability of detection, but also reduced the FA rate by 75% at the 90% probability of detection level. We later showed that this was an effective detection method in test data.

The spectrum-feature classifier rejected FAs by characterizing the spatial spectrum of the FAs. We showed that we could build a classifier that performed effectively on both training and test data. Figure 8 shows that we achieved a FA rate of 0.03 FA/m^2 with a >90% probability of detection on both the training and testing data. This result was created by selecting a set of 4 spectrum-features (from a possible 50) that allowed for a more generalized FA spatial spectrum model. A generalized classifier is an important aspect of a system that will be effective in an operational environment.

In the future we will examine ways in which our algorithm can be tuned to different types of explosive hazards. For example, different FLGPR center frequencies and bandwidths and spectrum-features may be optimal for different types of targets. Finally, the methods described in this paper used the FLGPR to detect the targets and the spectrum to reduce the FAs. The ALARIC system also contains an imaging system. We believe that images could be used in tandem with the FLGPR to detect targets, and we have already begun work in this realm.[18,19] We are also examining the fusion of cross-platform sensors to improve the detection / FA rate performance. Overall, we believe that the fusion of the FLGPR- and image-based explosive hazards detection approaches will show promise for significantly contributing to the remediation of the explosive hazards threat.

ACKNOWLEDGEMENTS

This work was supported by grants from the Leonard Wood Institute (LWI 181-222) and Army Research Office (48343-EV) in support of the U.S. Army RDECOM CERDEC NVESD.

REFERENCES

[1] Cremer, F., Schavemaker, J.G., de Jong, W., and Schutte, K., "Comparison of vehicle-mounted forward-looking polarimetric infrared and downward-looking infrared sensors for landmine detection", Proc. SPIE 5089, 517-526 (2003).
[2] Playle, N., Port, D.M., Rutherford, R., Burch, I.A., and Almond, R., "Infrared polarization sensor for forward-looking mine detection", Proc. SPIE 4742, 11-18 (2002).
[3] Costley, R.D., Sabatier, J.M., and Xiang, N., "Forward-looking acoustic mine detection system", Proc. SPIE 4394, 617-626 (2001).
[4] Collins, L.M., Torrione, P.A., Throckmorton, C.S., Liao, X., Zhu, Q.E., Liu, Q., Carin, L., Clodfelter, F., and Frasier, S., "Algorithms for landmine discrimination using the NIITEK ground penetrating radar", Proc. SPIE 4742, 709-718 (2002).
[5] Gader, P.D., Grandhi, R., Lee, W.H., Wilson, J.N., and Ho, K.C. "Feature analysis for the NIITEK ground penetrating radar using order weighted averaging operators for landmine detection", Proc. SPIE 5415, 953-962 (2004).
[6] Bradley, M.R., Witten, T.R., Duncan, M., and McCummins, R., "Anti-tank and side-attack mine detection with a forward-looking GPR", Proc. SPIE 5415, 421-432 (2004).
[7] Cosgrove, R.B., Milanfar, P., and Kositsky, J., "Trained detection of buried mines in SAR images via the deflection-optimal criterion", IEEE. Trans. Geoscience and Remote Sensing 42(11), 2569-2575 (2004).
[8] Sun, Y., and Li, J., "Plastic landmine detection using time-frequency analysis for forward-looking ground-penetrating radar", Proc. SPIE 5089, 851-862 (2003).
[9] Stone, K., Keller, J.M., Ho, K.C., and Gader, P.D. "On the registration of FLGPR and IR data for the forward-looking landmine detection system and its use in eliminating FLGPR false alarms," Proc. SPIE 6953, (2008).
[10] Havens, T.C., Stone, K., Keller, J.M., and Ho, K.C. "Sensor-fused detection of explosive hazards", Proc. SPIE 7303, 73032A (2009).

[11] Havens, T.C., Spain, C.J., Ho, K.C., Keller, J.M., Ton, T.T., Wong, D.C., and Soumekh, M., "Improved Detection and False Alarm Rejection Using FLGPR and Color Imagery in a Forward-Looking System", Proc. SPIE, (2010).
[12] Auger, A. and Hansen, N., "A Restart CMA Evolution Strategy with Increasing Population Size", Evolutionary Computation 2, 1769-1776 (2005).
[13] Hansen, N., Ostermeier, A., "Completely Derandomized Self-Adaptation in Evolution Strategies", Evolutionary Computation 9(2), 159-195 (2001).
[14] Hansen, N., "The CMA Evolution Strategy: A Tutorial", http://www.bionik.tu-berlin.de/user/niko/cmatutorial.pdf (2007).
[15] Wang, T., Sjahpetura, O., Keller, J.M., and Gader, P.D., "Landmine detection using forward-looking GPR with object-tracking," Proc. SPIE 5794, 1080-1088 (2005).
[16] Theodoridis, S., Koutroumbas, K., [*Pattern Recognition* (3rd ed.)], Academic Press, San Diego, CA (2006).
[17] Duda, R.O, and Hart, P.E., [*Pattern Classification and Scene Analysis*], John Wiley & Sons Inc. (1973).
[18] Keller, J.M., Stone, K., Ho, K.C., and Popescu, M., "Automatic cuing of human-in-the-loop detection system," Proc. SPIE 7303, 73032C (2009).
[19] Stone, K., Keller, J.M., Popescu, M., Havens, T.C., and Ho, K.C., "Forward looking anomaly detection via fusion of infrared and color imagery," Proc. SPIE, (2010).